RESTORING FORCE CHARACTERISTICS OF RC COLUMNS WITH HIGH-STRENGTH CONCRETE AND STEEL BARS UNDER AXIAL TENSION FORCE

Yuji Ishikawa[1], Hideki Kimura[2] and Masayuki Yamamoto[3]

[1] *Chief Researcher, Structural Engineering Section, Takenaka Research & Development Institute, Japan*
[2] *Senior Manager, Head Office, Takenaka Corporation, Tokyo, Japan*
[3] *Senior Manager, Building Design department, Tokyo Main Office, Takenaka Corporation, Japan*
Email: ishikawa.yuuji@takenaka.co.jp

ABSTRACT :

This research discusses the restoring forces characteristics of RC columns under axial tension force. This paper presents the review of typical experimental data and proposes a restoring force characteristics model of RC columns with high strength concrete and high strength steel bars under axial tension force. Fourteen RC column specimen tests were carried out under varying axial forces to simulate the case of lower story columns of high-rise RC buildings under earthquake loading with high strength concrete, over 100MPa, high strength steel fiber reinforced concrete up to 171MPa and high strength longitudinal bars up to 1201MPa. This research presents the restoring force characteristics model of a multi linear model connecting three characteristic points defined as the elastic breaking point, tensile flexural yielding point, and the R-20 strength points, with respect to the restoring force characteristics of the tested high-strength concrete columns under axial tension forces. The R-20 point is relative to the flexural strength at the drift angle -0.02 rad. It has been verified from the results that the restoring force characteristics of the model proposed in this research are applicable to properly assess the restoring force characteristics (at the drift angles up to -0.02 rad of high-strength (steel fiber) concrete columns under axial tension forces.

KEYWORDS: Reinforced concrete, Column, Axial tension force, Restoring force characteristics, High strength concrete, High strength steel

1. INTRODUCTION

In recent years, the aspect ratio of high-rise buildings, (building against its narrower length of building), tends to increase in Japan. Some of RC high-rise buildings with high aspect ratio will experience axial tension forces their columns under severe earthquakes. The restoring force characteristics of such columns are different from those of columns subjected to axial compression only. These properties greatly affect the seismic response analysis. Although some researches have been conducted on RC columns with varying axial force, no method has been derived to properly assess the restoring force characteristics under axial tension force, at present. Therefore, this research shows the features of the restoring force characteristics of RC column members under varying axial forces including axial tension forces.

2. TYPICAL EXPERIMENTAL RESULTS WITH HIGH STRENGTH MATERIALS

2.1. Outline of the experimental test

Our experimental studies were carried out to deepen the understanding of structural performance of RC columns using high strength materials under varying axial loads. The experimental tests focused on the structural performance of columns under tension axial forces to simulate the combined effect of horizontal and vertical components of actual earthquake loading. **Figure 1** shows the test specimen Unit 102 (a representative element of the 14 tested specimens) under a varying axial force that was proportioned to the shear force as shown in **Figure 1(c)**. High-strength concrete of 121.6MPa was used. High-strength steel bars SD685 (yield strength fy=709MPa which had a yield plateau, an elongation of 10.6% and a ratio of yield strength to maximum strength of 79%) was used for the longitudinal bars. **Figure 1(d)** shows the relationships of the shear force to the drift angle of the related specimen and **Figure 2** shows the developed crack patterns.

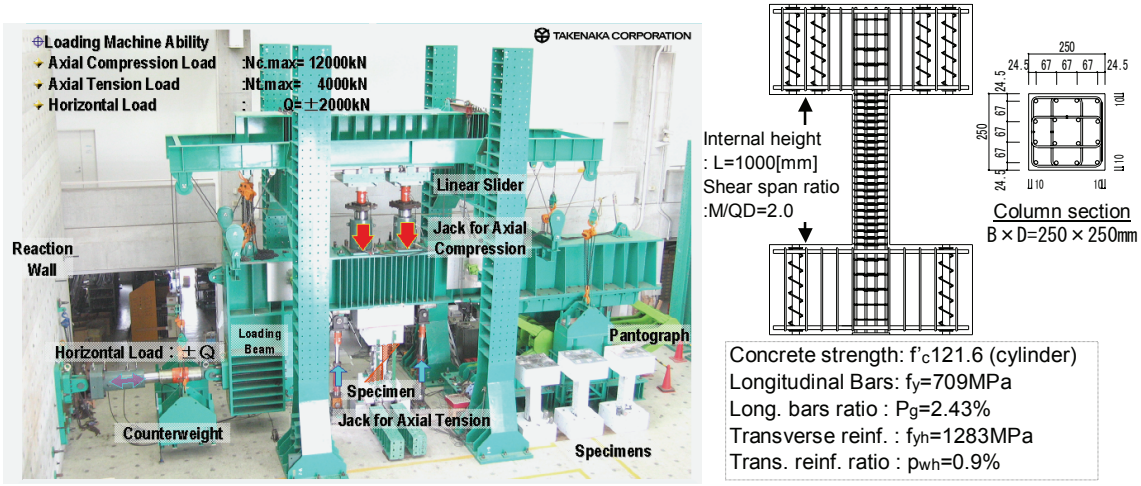

(a) Loading system (Double curvature type with varying axial force) (b) Specimen (Unit102)

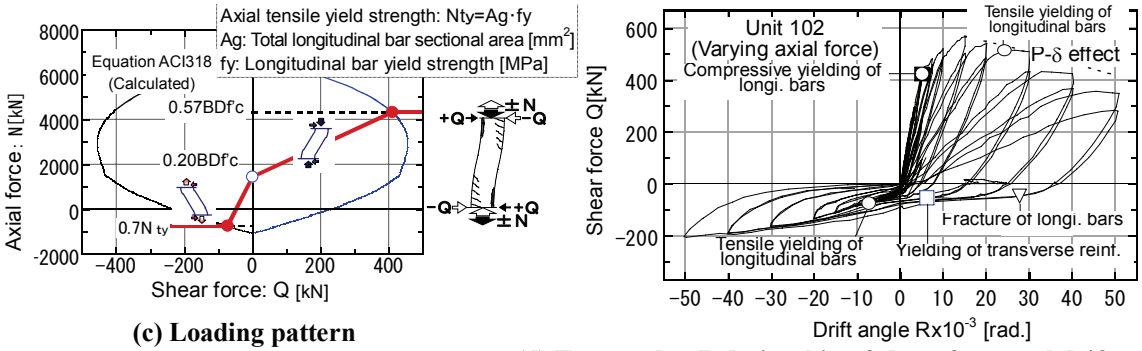

(c) Loading pattern (Relationship of Axial force and shear force) (d) Test results: Relationship of shear force and drift angle

Figure 1 Seismic performance of Unit 102, HSC columns under varying axial load

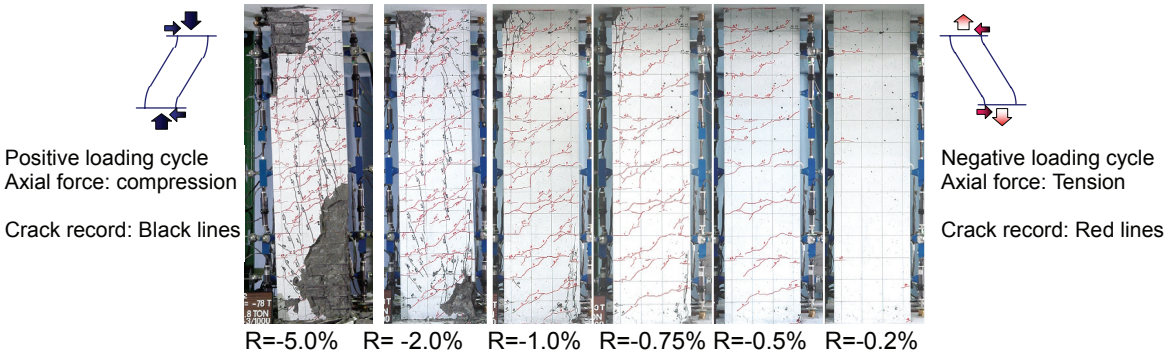

Figure 2 Typical crack patterns of HSC columns under varying axial load, Unit102

2.2 Experimental test results

For Unit 102, the crushed range of the compressed concrete expanded during the positive loading when axial compression forces acted after the shear strength reached the maximum at the drift angle of +15/1000 rad, and bar buckling was observed in some of the compression-side longitudinal bars at +50/1000 rad. After that, the longitudinal bars fractured during the transition to the negative loading with the axial tension force, when the test was terminated. The restoring force characteristics under axial tension forces showed that the stiffness decreased abruptly after the flexural crack was initiated at the drift angle -1.0/1000 rad and the longitudinal bars yielded during loading at the drift angle -7.5/1000 rad. At that moment, however, the stiffness did not decrease abruptly, and the strength gradually increased with the increase of deformation even after yielding. Figure 2 shows successive crack patterns. The flexural cracking started at the drift angle of –1/1000 rad. The crack

pattern relative to the drift angle -7.5/1000 rad corresponds to the time of longitudinal bar's yielding; and the photo of the drift angle -50/1000 rad shows the pattern at the maximum deformation. The concrete damage, recognizable in the lower right and upper left of the photos of the crack patterns, happened when the axial load was on the compression side (positive loading), and the crushed range expanded as the deformations increased. The concrete damage grew only on the positive loading side where the axial compression force increased with the shear force, while the concrete damages in negative loading with the axial tension forces were comparatively minor. Nevertheless, at the drift angle -7.5/1000 rad, when the tensile flexural yielding was reached, the flexural cracks developed across the whole length of the column while simultaneously transiting to flexural shear cracks. The range of such transition points from the flexural cracks to the flexural shear cracks was equivalent to the range that connects the compression regions of the top and bottom critical sections.

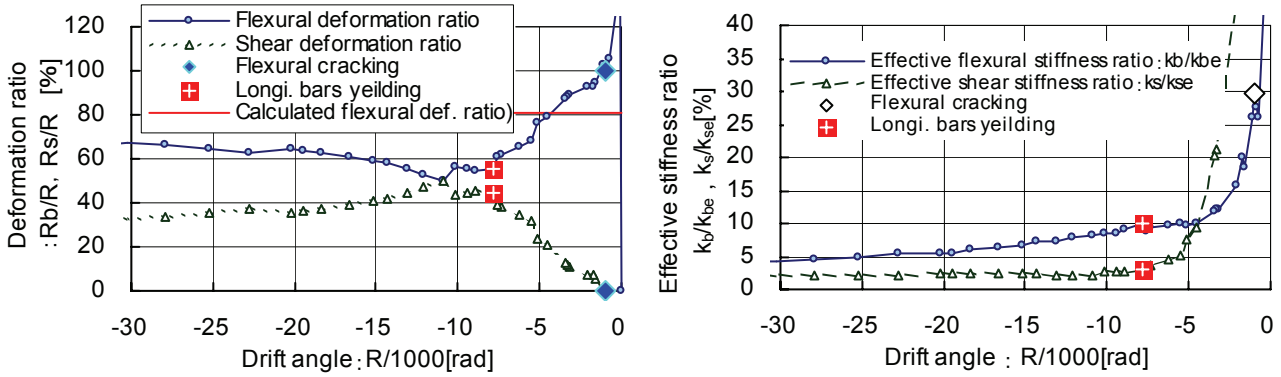

(a) Flexural deformation and shear deformation ratios (b) Effective flexural and shear stiffness ratios

Figure 3 Transitions of deformation ratios and effective stiffness ratios of Unit 102

2.3 Consideration of the experimental tests

Figures 3(a) shows the ratios of flexural and shear deformations to the total deformation. It can be confirmed that the flexural deformation was dominant before the flexural cracking point. After the flexural cracking, the flexural deformation ratio abruptly decreased and went even below the calculated values in an elastic condition. Shear deformation ratio was calculated by subtraction of the flexural deformation from the whole deformation. **Figure 3(b)** shows the variation of the effective flexural stiffness ratio (k_b/k_{be}), and the effective shear stiffness ratio (k_s/k_{se}). After the flexural cracking point, the effective flexural and shear stiffness ratios abruptly decreased and caused the longitudinal bars to reach yielding. It can be seen that such decrease of effective shear stiffness as well as effective flexural stiffness is a feature of RC columns under axial tension forces, and it is considered to be caused by a series of process in which flexural cracks developed almost horizontally across almost the whole length of the column as shown in **Figure 2**. By comparison to non-cracked concrete, it seems that the shear stiffness of the column member decreases because the shear stiffness on the cracked surface decreases.

3. PRINCIPALE OF MODELING AND DEFINITION OF CHARACTERISTIC POINTS

In this research, the restoring force characteristics of RC columns under axial tension forces were modeled by using three characteristic points as shown in **Figure 4.** These characteristic points were as follows.

1) Elastic breaking point under axial tension force (R_{tse}, Q_{tse})
This characteristic point defines the elastic breaking point under axial tension force when flexural cracks develop. The measured data has been analyzed as to the relationship between the measured secant elastic stiffness ($_{ex}k_{tse}$) and the calculated elastic stiffness equivalent to the initial stiffness ($_{cal}k_e$). The proposed method assesses the secant stiffness at the elastic breaking point as the result of multiplying the calculated elastic stiffness by the secant modulus of tension (ϕ_{te}) equivalent to a correction coefficient.

2) Tensile flexural yielding point (R_{ty}, Q_{ty})
After elastic breaking point, the subsequent tangential stiffness becomes almost constant for RC columns under axial tension force. The tensile flexural yielding point is defined by the state at which the longitudinal bars yield. The proposed method defines the stiffness at the tensile flexural yielding point as the calculated

elastic stiffness by the decreasing rate of stiffness at the tensile flexural yielding point (α_{ty}).

3) R-20 strength point: the point at the drift angle (R) -20/1000 (R_{-20}, Q_{R-20})

The R-20 strength point of RC columns under axial tension force corresponds to the point of the drift angle -20/1000rad. This point was estimated by consideration of the strength enhancement due to the P-δ effect and the strain hardening of the longitudinal bars.

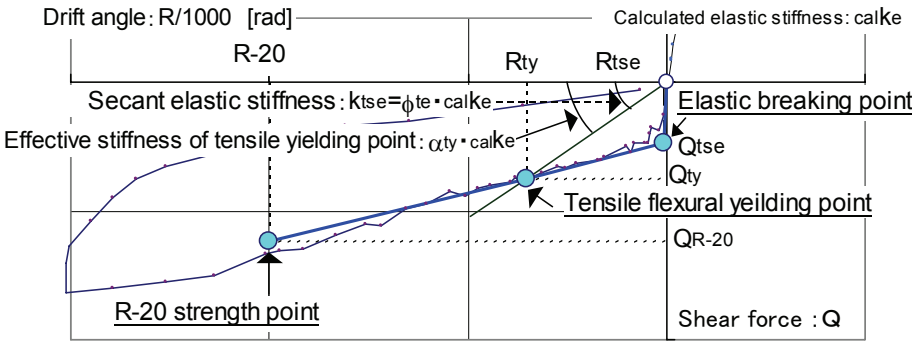

Figure 4 Modeling of restoring force characteristics under axial tension force

4. RESTORING FORCE CHARACTERISTICS UNDER AXIAL TENSION FORCES

Our studies were conducted on the measured data of tested column members under varying axial forces. Concrete strength of measured data ranged between f'_c56.8 and 148.6MPa, the longitudinal bar yielding strength ranged between 366 and 709MPa, and the axial tension force level (ratio of axial tension force to axial tensile yield strength) ranged between 0 and 0.85. Besides, our experimental data included columns with high strength steel fiber reinforced concrete, over 170MPa and high strength longitudinal bars, over 1200MPa (Hassane 2007).

4.1. Elastic breaking point (under axial tension forces)

The secant stiffness at the elastic breaking point was defined by providing the calculated elastic stiffness with the tensile secant modulus coefficient, ϕ_{te} , as given in **Eq.1**. The coefficient was obtained from the secant modulus under axial tension forces using basic data. As a result, this research gives the tensile secant modulus coefficient, ϕ_{te} the value 0.56. And, the strength relative to the elastic breaking point was calculated using the strength of material method. Nevertheless, the tensile concrete strength was defined as $0.313\sqrt{f'c}$, f'c : compressive concrete strength.

The secant elastic stiffness under axial tension force] $${}_{cal}k_{tse} = \phi_{te}\frac{1}{1/k_B + 1/k_S} \quad (1)$$

ϕ_{te} = 0.56 : Tensile secant modulus cofficient

k_B : Elastic flexural stiffness [kN/mm], k_S : Elastic shear stiffness [kN/mm]

4.2. Tensile flexural yield strength (under axial tension forces)

The tensile flexural yield strength was studied by using 14 measured data. To find the calculation values, the equation ACI318 (2002) was used. The mean of the ratios of measured to calculated values was 0.95. It has been confirmed that all the measured data of strengths at the tensile flexural yielding points can be estimated within the range of ±30%. The coefficient variation was 11.3%.

4.3. Effective stiffness under axial tension force at tensile flexural yielding point

4.3.1 Outline of proposed macro model of the effective stiffness under axial tension forces

The effective stiffness under axial tension force means the secant stiffness at tensile flexural yielding point. The macro model under axial tension forces was defined as shown in **Figure 5**, derived from our experimental observations**.** In the proposed macro model, the region that connects the compression regions of the top and bottom critical sections at the tensile flexural yielding point was defined as the region effective in flexural shear

stiffness, where the concrete effective geometrical moment of inertia changes in the direction parallel to the axis of member. Derived from the function of that effective geometrical moment of inertia in the direction parallel to the axis of member and the distance from the inflection point, the differential equation of deflection pertinent to the flexural deformation at the tensile flexural yielding point was constructed, from which the stiffness at the tensile flexural yielding point was calculated. In the procedure, however, the effective Young's modulus of concrete was defined in accordance with the analysis of the measured data presented in *4.3.3*, considering that the Young' modulus of concrete might be lowered due to the cracks that would propagate over the assumed effective sectional region of concrete, where the reinforcement's geometrical moment of inertia should be the same as in an elastic condition. The shear stiffness at the tensile flexural yielding point was also defined by using the effective section and effective Young's modulus of concrete. For the effective geometrical moment of inertia at the tensile flexural yielding point, the compression regions of the top and bottom critical sections (section A-A') under double curvature flexural moment and axial tension forces were defined by the ultimate flexural strength of the equation ACI318-02 as shown in **Figure 5**. Nevertheless, in this research, the concrete strain at the extreme compression fiber for high-strength concrete was evaluated using **Eqn.2**, which was deduced from experimental data.

Concrete strain at extreme compression fiber: ε_u (Ishikawa 2002)

$$f'c \leqq 55 \quad \varepsilon_u = 0.003, \quad 55 \leqq f'c \leqq 110 \quad \varepsilon_u = 0.003 + 0.0001816\,(f'c - 55)\,, \quad 110 \leqq f'c \quad \varepsilon_u = 0.004 \tag{2}$$

The ratio of the neutral axis depth to the column section depth, representing the size of the compression region, was defined as the effective section-depth ratio (α_t). The effective geometrical moments of inertia of the critical section A-A', the section B-B' at the inflection point, and the section separated by the distance from the inflection point, x, can be found using the equations shown in **Figure 5**.

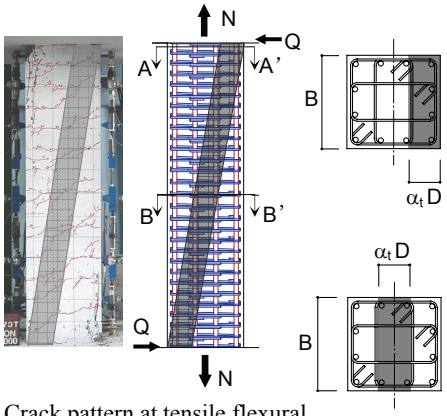

Crack pattern at tensile flexural yielding and proposed macro model

(Section A-A': Critical section)
Effective geometrical moment of inertia

$$I_{A-A'} = \frac{B(\alpha_t D)^3}{12} + B\alpha_t D \times \left(\frac{D}{2} - \frac{\alpha_t D}{2}\right)^2 + Ist$$

* Shaded area: Compression region,
I_{st}: Geometrical moment of inertia only of reinforcement,
α_t: Effective section-depth ratio,
B: Column section width, D: Section depth, L_o : Clear height of column

$$I_{B-B'} = \frac{B(\alpha_t D)^3}{12} + Ist$$

(Section B-B': Inflection point)
Effective geometrical moment of inertia

Figure 5 Proposed macro model of the effective stiffness at tensile flexural yielding under axial tension forces

Effective geometrical moment of inertia of section separated by x from inflection point: I_t

$$I_t = \frac{BD^3}{12}\alpha_t^{\,3} + \frac{BD^3\alpha_t \times (1-\alpha_t)^2}{Lo^2}x^2 + I_{st} \tag{3}$$

4.3.2 Flexural deformation and flexural stiffness reduction ratio at tensile flexural yielding point

The flexural deformation at the tensile flexural yielding point, based on the effective geometrical moment of inertia given in **Eqn. 3**, can be derived by considering the initial conditions into the differential equation of deflection, **Eqn. 4**. And then, assuming that the flexural stiffness is an elastic flexural stiffness, the deformation is calculated as the elastic flexural deformation **Eqn. 7.**

$${}_t\delta_{by} = \int {}_t\theta_{by}\,dx = \iint \frac{M_{ty}}{E_t I_t}dx + \iint \frac{M_{ty}}{E_s I_{st}}dx \tag{4}$$

$${}_t\theta_{by} = \int \frac{Q_{ty}\cdot x}{E_t\left\{\frac{BD^3}{12}\alpha_t^{\,3} + \frac{BD^3\alpha_t(1-\alpha_t)^2}{Lo^2}x^2\right\}}dx + \int \frac{Q_{ty}\cdot x}{E_s I_{st}}dx \tag{5}$$

Flexural deformation ($_t\delta_{by}$) and flexural elastic deformation ($_t\delta_{be}$) at tensile flexural yielding point

When the distance from the inflection point is $x = L_o/2$, from ${}_t\theta_{by} = 0$, ${}_t\delta_{by} = 0$,

$$\therefore {}_t\delta_{by} = \frac{QtyLo}{2EtBD^3\alpha t(1-\alpha t)^2}\left\{x\log\left|x^2+\frac{\alpha t^2 Lo^2}{12(1-\alpha t)^2}\right| - 2x\frac{\alpha tLo}{\sqrt{3}(1-\alpha t)}\tan^{-1}\left(\frac{2\sqrt{3}(1-\alpha t)x}{\alpha tLo}\right)\right.$$

$$\left. - x\log\left|\frac{Lo^2}{4}+\frac{\alpha t^2 Lo^2}{12(1-\alpha t)^2}\right| + Lo - \frac{\alpha tLo}{\sqrt{3}(1-\alpha t)}\tan^{-1}\left(\frac{2\sqrt{3}(1-\alpha t)x}{\alpha tLo}\right)\right\} + \frac{Qty\cdot x^3}{6EcIst} \quad (6)$$

The effective stiffness reduction ratio of flexural deformation : $\alpha_{tb} = \dfrac{{}_t\delta_{be}}{{}_t\delta_{by}}$, ${}_t\delta_{be} = Q_{ty}/k_B$ (7)

$_t\delta_{by}$: Flexural deformation at tensile flexural yielding point
$_t\theta_{by}$: Flexural rotation angle at tensile flexural yielding point
E_t : Effective Young's modulus of concrete at tensile flexural yielding point (Eqn.8)
E_c : Young's modulus of concrete
E_s : Young's modulus of reinforcement
I_t : Effective geometrical moment of inertia at tensile flexural yielding point
I_{st}: Geometrical moment of inertia only of longitudinal bars (ratio of Young's modulus considered)
M_{ty},Q_{ty}: Strength at tensile flexural yielding point (in terms of bending moment, shear force)
α_t : Effective section-depth ratio at tensile flexural yielding point (=Neutral axis depth ratio of critical section)

4.3.3 Effective Young's modulus of concrete under axial tension forces (E_t)

At the tensile flexural yielding point, cracks expand into the assumed effective sectional region of concrete, where the Young's modulus of concrete decreased as the crack widths opened and closed. This effective Young's modulus of concrete decreases as the axial tension force increases because the crack widths increase according to the magnitude of axial tension forces. For the effective Young's modulus of concrete at the tensile flexural yielding point, Eqn. 8 was introduced here as an evaluation formula that represents the decrease in the secant stiffness of concrete with the expansion of crack widths caused by the increase of axial tension forces. Eqn. 9 gives the strain corresponding to the compressive strength were calculated by means of (Ishikawa 2002).

Effective Young's modulus of concrete under axial tension force (E_t)

$$E_t = \frac{\varepsilon_m}{\varepsilon_m - \varepsilon_t}E_c \quad (8)$$

$$\varepsilon_m = \left(18.684\times f'_c + 1514.2\right)\times 10^{-6}, \quad \varepsilon_t = \frac{N_t}{A_g E_s} \quad (9)$$

ε_m: Concrete strain at compressive strength, ε_t : Reinforcement strain caused by axial tension force
N_t: Axial tension force , A_g : Sectional area of reinforcement

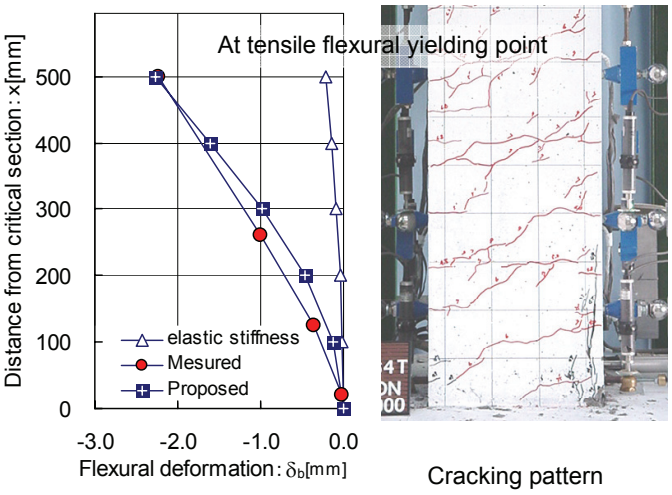

Figure 6. Verification example of flexural deformation distribution at tensile flexural yielding point (Unit 102)

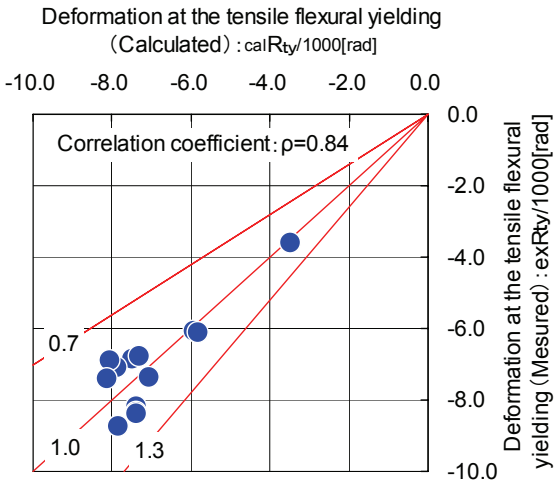

Figure 7. Comparison of deformations at tensile flexural yielding points

4.3.4 Flexural deformation distribution at tensile flexural yielding point

Figure 6 shows a comparison between the measured and calculated values of flexural deformation distribution, using the typical measured data of Unit102 (refer to section **2.**) in order to check the validity of the flexural deformations of the tensile flexural yielding point as given the proposed **Eqn. 6** and the effective Young's modulus of concrete in **Eqn. 8**. The flexural deformations in **Figure 6** are shown on the assumption that the deformation at the critical section position is the original point. The same figure shows the flexural deformation distribution due to the elastic flexural stiffness (Eqn. 1) for reference as well. Although there is a slight difference between the shapes of the flexural deformation distributions, the flexural deformations are properly assessed, which indicating the validity of **Eqn. 6** and **Eqn. 8**.

4.3.5 Shear stiffness reduction factor at tensile flexural yielding point, and study case

The shear stiffness at the tensile flexural yielding point was assessed by assuming the effective section as in **Figure 4** in the same manner as the macro model assumed in the calculation of flexural stiffness and multiplying the shear stiffness in an elastic condition by the area ratio of the effective section equivalent to the compression region to the whole section and the effective ratio of Young's modulus. The proposed shear stiffness is shown in **Eqn. 10**, and the shear stiffness reduction factor is shown in **Eqn.11**.

Elastic shear stiffness (k_{se}), Effective shear stiffness (k_{ts}) and shear stiffness reduction ratio (α_{ts}) at tensile flexural yielding point:

$$k_{se} = \frac{G \cdot B \cdot D}{\kappa L_o} = \frac{Ec \times B \cdot D}{2(1+\nu)\kappa L_o},\ k_{ts} = \frac{G_t \cdot B \cdot \alpha_t D}{\kappa L_o} = \frac{E_t \times B \cdot \alpha_t D}{2(1+\nu)\kappa L_o},\ \text{Poisson's ratio}: \nu = 0.0006f'c + 0.14 \quad (10)$$

$$\therefore \alpha_{ts} = \frac{k_{ts}}{k_{se}} = \frac{E_t}{E_c} \times \alpha_t \quad (11)$$

4.3.6 Stiffness reduction factor at tensile flexural yielding point

The stiffness at tensile flexural yielding point (k_{ty}) and the stiffness reduction factor at tensile flexural yielding point (α_{ty}) can be calculated as follows, by using the flexural stiffness reduction factor at tensile flexural yielding point (α_{tb}; **Eqn. 7**) and the shear stiffness reduction factor at the same point (α_{ts}; **Eqn. 11**).

Stiffness reduction factor at tensile flexural yielding point (α_{ty})

$$\alpha_{ty} = \frac{k_{ty}}{k_e},\quad k_{ty} = \frac{1}{\left(\frac{1}{{}_t k_{by}} + \frac{1}{{}_t k_{sy}}\right)},\quad {}_t k_{by} = \alpha_{tb} k_{be},\quad {}_t k_{sy} = \alpha_{ts} k_{se} \quad (12)$$

k_{ty} : Parallel sum of flexural stiffness and shear stiffness at tensile flexural yielding point

k_e : Parallel sum of elastic flexural stiffness and elastic shear stiffness

α_{tb} : Flexural stiffness reduction factor at tensile flexural yielding point

α_{ts} : Shear stiffness reduction factor at tensile flexural yielding point

Deformation at tensile flexural yielding point (δ_{ty})

$$\delta_{ty} = Q_{ty} / k_{ty} \quad (13)$$

Q_{ty} : Strength at tensile flexural yielding point (ACI318-02)

Where, the concrete strain at the extreme compression fiber should be as defined in Eqn.4.

4.4 Verification of the deformation at tensile flexural yielding point

Figure 7 shows a comparison between the measured and calculated values in terms of the deformation at tensile flexural yielding point (**Eqn.13**). It was verified that all specimens of measured data could be properly assessed at the precision within ±30%. The mean and variation coefficient of the ratios between measured and calculated values were 1.02 and 9.7%, respectively. This result showed that the proposed model is able to estimate the restoring force characteristics of RC columns using high strength materials under axial tension force.

4.5 Assessment of the R-20 strength point

The strength of RC columns under axial tension forces continues to increase with the increase of the drift angles after the longitudinal bars have yielded. The R-20 strength point was estimated by means of the assuming

method that the plastic hinges at the member ends when the drift angle is -20/1000 rad. The R-20 strength was found by calculating the rise of the longitudinal bars' stress by means of the strain hardening which was calculated by the Menegotto-Pinto model modified (Ciampi 1982) and adding the additional bending moment due to the P-δ effect. For a more details about the method can be found in Ishikawa, 2004.

5. VERTIFICATION OF PROPOSED EQUATIONS

A case of the comparison between the restoring force characteristics model under the axial tension forces of RC columns using the high-strength materials proposed here, and the measured values is shown in **Figure 8**. **Figure 8(a)** shows the verification result on HSC column of the Unit 102 described in section **2**. The proposed model and the test results indicate that the equations reproduced the test results properly until the point of the R-20 strength. **Figure 8(b)** shows the verification result on the high-strength steel fiber reinforced concrete column of the Unit701 (Hassane 2007). Unit701 had a high strength concrete of 171MPa and the restoring force characteristics of the proposed equations also reproduced the test results accurately..

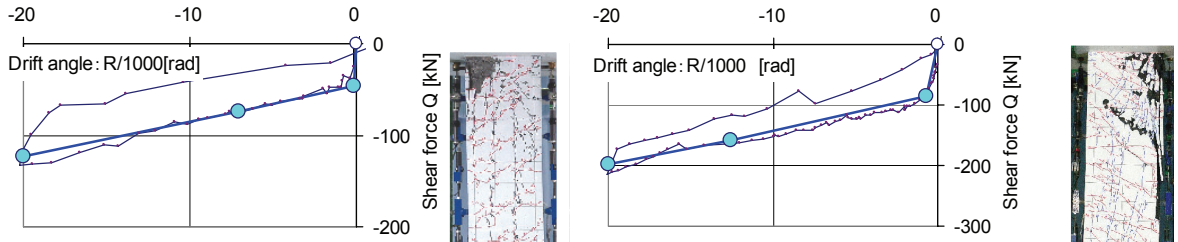

(a) Unit 102: HSC column

Varying axial loading	
Axial compression force level	ηc=0.57~
Axial tension force level	ηt =~-0.7
Concrete compressive strength	f'c121. 6MPa
Longitudinal bars yield strength	fy=709MPa

(b) Unit 701: HSFR column

Varying axial loading	
Axial compression force level	ηc=0.60~
Axial tension force level	ηt =~-0.7
Concrete compressive strength	f'c171MPa
Longitudinal bars yield strength	fy=1201MPa

Figure 8. Comparison of restoring force characteristics under axial tension forces between measured data and proposed equations

6. Conclusion

This research proposes the restoring force characteristics model of a multi linear model connecting three characteristic points defined as the elastic limit point, tensile flexural yielding point, and the R-20 strength points, with respect to the restoring force characteristics of the high-strength-material column members under axial tension forces. The adequacy of the proposed model was verified by using measured data of 14 column specimens with the concrete strength between 56.8 and 148.6MPa, the longitudinal bar yielding strength between 366 and 709MPa, and the axial tension force levels between 0 and 0.85. The proposed model was confirmed to be appropriate for high strength steel fiber reinforced concrete columns with high strength concrete up to 171MPa and high strength longitudinal bars of yield strength up to 1201MPa.

REFERENCES

1) Ishikawa, Y. (2002). Restoring Force Characteristics of Column Members Using High-strength Materials, Dissertation, University of Tokyo.
2) Ishikawa, Y, Kimura, H. (2004), Restoring force characteristics of R/C columns with high strength concrete and steel under axial tension force, *Journal of Structural Engineering*, Vol.50B, 47-58
3) American Concrete Institute (2002), Building Code Requirements for Structural Concrete (318-02) and Commentary (318R-02).
4) Ciampi, V. et al., (1982). Analytical Model for Concrete Anchorages of Reinforcing Bars under Generalized Excitations, *Report No. EERC-82/23*, Univ. of California.
5) Hassane, O et al., (2007). Seismic Performance of Ultra-high-strength Concrete Columns using High strength Longitudinal Bars, *Proceeding of the Japan Concrete Institute*, Vol. 29, No.3, 134-140